Research in Astronomy and Astrophysics, 22:025010 (10pp), 2022 February https://doi.org/10.1088/1674-4527/ac3e5c

Number and Distribution of Fiducial Fibers in a Spectroscopic Survey Telescope

Shi-Peng Duan[1], Zeng-Xiang Zhou[1,5,*], Jia-Le Zuo[1], Meng-Tao Li[1], Zhi-Gang Liu[1], Hong-Zhuan Hu[1], Jian-Ping Wang[1], Xiang-Qun Cui[2,3], Yong Zhang[2,4], and Hao-Tong Zhang[4]
[1] Department of Precision Machinery and Precision Instrumentation, University of Science and Technology of China, Hefei 230026, China; zzx@ustc.edu.cn
[2] National Astronomical Observatories/Nanjing Institute of Astronomical Optics & Technology, Chinese Academy of Science, Nanjing 210042, China
[3] CAS Key Laboratory of Astronomical Optics & Technology, Nanjing Institute of Astronomical Optics & Technology, Nanjing 210042, China
[4] National Astronomical Observatories, Chinese Academy of Sciences, Beijing 100012, China
Received 2021 July 9; revised 2021 October 28; accepted 2021 November 9; published 2022 February 2

Abstract

To date, the Large Sky Area Multi-Object Fiber Spectroscopic Telescope (LAMOST) has been in operation for 12 yr. To improve the telescope's astronomical observation accuracy, the original open-loop fiber positioning system of LAMOST is in urgent need of upgrading. The upgrade plan is to install several fiber view cameras (FVCs) around primary mirror B to build a closed-loop feedback control system. The FVCs are 20 m from the focal surface. To reduce a series of errors when the cameras detect the positions of the optical fibers, we designed fiducial fibers on the focal surface to be fiducial points for the cameras. Increasing the number of fiducial fibers can improve the detection accuracy of the FVC system, but it will also certainly reduce the number of fiber positioners that can be used for observation. Therefore, the focus of this paper is how to achieve the quantity and distribution that meet the requirements of system detection. In this paper, we introduce the necessity of using fiducial fibers, propose a method for selecting their number and present several methods for assessing the uniformity of their distribution. Finally, we implement particle swarm optimization to find the best distribution of fiducial fibers.

Key words: instrumentation: detectors – techniques: image processing – methods: data analysis – telescopes

1. Introduction

In the early design stage of the Large Sky Area Multi-Object Fiber Spectroscopic Telescope (LAMOST), Xing et al. (1998) proposed the new idea of an optical fiber (OF) positioning scheme characterized by independent positioning and parallel control of multi-target OFs. After this, improvements to the OF control actuator (Hu et al. 2003) along with the final implementation scheme (Hu et al. 2006) were proposed, and the automatic OF positioner was successfully implemented. In the United States, the Dark Energy Spectroscopic Instrument (DESI) also uses an independent control scheme like LAMOST, which is achieved with robots (with Θ-Φ motors, Θ represents the central axis, Φ represents the eccentric axis.) moving in parallel (Schubnell et al. 2016), and experiments have demonstrated its feasibility (Horler et al. 2018). The MEGARA of the Gran Telescopio Canarias 10.4-m telescope in Spain also relies on multi-target fiber positioning technology in multi-object spectrograph (MOS) mode (Pérez-Calpena et al. 2018), and the Cobra positioner utilized by the Subaru Telescope in Hawaii has a similar structure (Fisher et al. 2012). With the increasing demand for OF spectral investigations, OF independent positioners are being increasingly utilized in OF spectral telescopes.

The OF positioner in LAMOST has 4000 OF positioning robots located on the focal surface that can be used to capture the light of stars or galaxies. Each fiber is installed on a small, high-precision positioning robot (Hu et al. 2016), and the accurate positioning of the OFs ensures the spectral quality of the received light.

The open-loop control method (Cui et al. 2012) that LAMOST uses currently requires maintenance of all the fiber positioners from June to July each year. In this process, first, we install a CCD camera 1 m in front of the focal surface and calibrate the camera with a standard target (Liu et al. 2011). Then, the motion of the positioner is captured by the CCD camera and its error curve is calculated. The two-dimensional error curve of each OF positioner is recorded. In observation, the motion accuracy of the OF positioner is corrected by the error curve obtained in advance. This method only relies on mechanical accuracy and cannot detect the movement state or correct the positioner operation errors in real time.

In 2020–2022, the telescope upgrade project plans to add six fiber view cameras (FVCs) in LAMOST to locate the OFs and update the positioning mode to a closed-loop design with position feedback; that is, the motors on the OF positioner are

* Corresponding author.
[5] These authors contributed equally to this work.

first controlled to run once, after which the OFs are measured by photography to see whether the positioner accurately controls them to reach their target positions. If not, the pulse compensation required for motor operation is calculated by a visual positioning system. After repeating this twice, the OFs finally reach their target positions. In this closed-loop positioning mode, it is necessary to ensure the shooting accuracy of the camera. At present, the zero position of the OF positioner used in LAMOST is the hardware contact point, and the repeated zero return precision is 2 μm. To improve the accuracy and efficiency of OF positioning and to meet the needs of closed-loop positioning, the next generation of OF positioner (Hu et al. 2018) will be improved with a smaller no-zero-position design.

In closed-loop positioning mode, for real-time positioning of the OFs, six FVCs are installed around primary mirror B at 20 m from the focal surface. Each camera covers one-sixth of the focal surface. Because of the long distances between FVCs and the focal surface, air and other environmental disturbances have a great influence on the OF repeatability. Therefore, a certain number of fiducial fibers (FFs) must be distributed on the focal surface to provide fixed fiducials for visual positioning and to correct the FVC errors. In the FF design, each FF unit occupies one OF positioner location. The increased number of FFs means that fewer OF positioners are available for operation. Therefore, the main focus here is how to determine the minimum number of FFs for the required accuracy of system visual detection. Additionally, the focal-plane center of the LAMOST telescope contains a Shack-Hartmann wave front sensor and four guider CCDs, and the area occupied by these devices in the focal surface should be considered in the FF distribution. This means that the FF distribution cannot be a simple uniform case while also providing the optimal solution for six camera zones and the image mosaic. Therefore, we seek the optimal solution for the FF distribution.

Starting in 2019, the DESI project installed 100 illuminated fiducials for fiber positioning (Aghamousa et al. 2016). Similarly, the Prime Focus Spectrograph of the Subaru Telescope was also mentioned using FFs for fiber positioning (Fisher et al. 2014). In essence, FFs are calibration tools that can provide accurate positioning.

The remainder of this paper is organized as follows. In Section 2, we compare experimental results for the repeatability of shooting the working OFs in LAMOST with that of shooting a standard target in the laboratory, which shows the necessity of using high-precision FFs. In Section 3, we demonstrate how the number of FFs influences the repeatability error; through experiments with different systematic errors and random errors, we propose a method for determining the number of FFs. In Section 4, we describe how the FF distribution influences the repeatability error and explore how to distribute the FFs reasonably; we use particle swarm optimization (PSO) and Voronoi diagrams to find a reasonable distribution. In Section 5, we explore future application prospects and analyze some of the deficiencies of our method.

2. Necessity of Using Fiducial Fibers

Polynomial fitting gives rapid calibration results and guaranteed calibration accuracy (Tang et al. 2017). Currently, LAMOST uses fourth-order polynomial fitting to calibrate the camera (Liu et al. 2011) and utilizes the light center-of-gravity method (Zhao et al. 2018a) to identify the OF positions under back illumination (Zhou et al. 2016). The expressions for this are

$$x_{\rm img} = \frac{\sum_{i=0}^{n}(G(x_i, y_i) - T)^2 \times x_i}{\sum_{i=0}^{n}(G(x_i, y_i) - T)^2},$$
$$y_{\rm img} = \frac{\sum_{i=0}^{n}(G(x_i, y_i) - T)^2 \times y_i}{\sum_{i=0}^{n}(G(x_i, y_i) - T)^2} \quad (1)$$

where n is the number of pixels occupied by the light spot, $G(x_i, y_i)$ is the gray value of each pixel, T is the gray value of the background and $(x_{\rm img}, y_{\rm img})$ is the fiber position that is finally obtained.

However, we do not have the exact coordinates of the actual positions for use in the polynomial fitting. Currently, all we can consider are the coordinates of the machining holes in the focal surface as the theoretical coordinates of the OF positioners in the zero position. However, those coordinates are not accurate because the holes in the focal surface and the OFs on the positioners are not in the same plane. The distance between the focal surface and an OF is 120 mm, and so the coordinates of the holes in the focal surface are not a good representation of those of the OFs.

To explore how the positioning accuracy is affected by using the hole coordinates as the theoretical OF coordinates, we designed a control experiment to compare the repeatability accuracy of the LAMOST OFs with that of a standard target in the laboratory.

2.1. Repeatability Experiment with LAMOST Fibers

Figure 1(a) depicts the LAMOST focal surface. Currently, six CMOS FVCs with 6k × 8k resolution are used for OF positioning (Zhao et al. 2018b). Figure 1(b) depicts the field of view (FOV) division of the six cameras; to prepare for the subsequent FOV splicing, each adjacent pair has an overlapping area.

In the experiment, we used the FVC with the FOV numbered 5 in Figure 1(b) (hereinafter referred to as FVC5), and all the OF positioners were in their zero positions. We used FVC5 to shoot for 30 minutes, once per second, with a total of 1800 images taken. Fitting with a fourth-order polynomial requires 30 calculation parameters; however, the FOV of FVC5

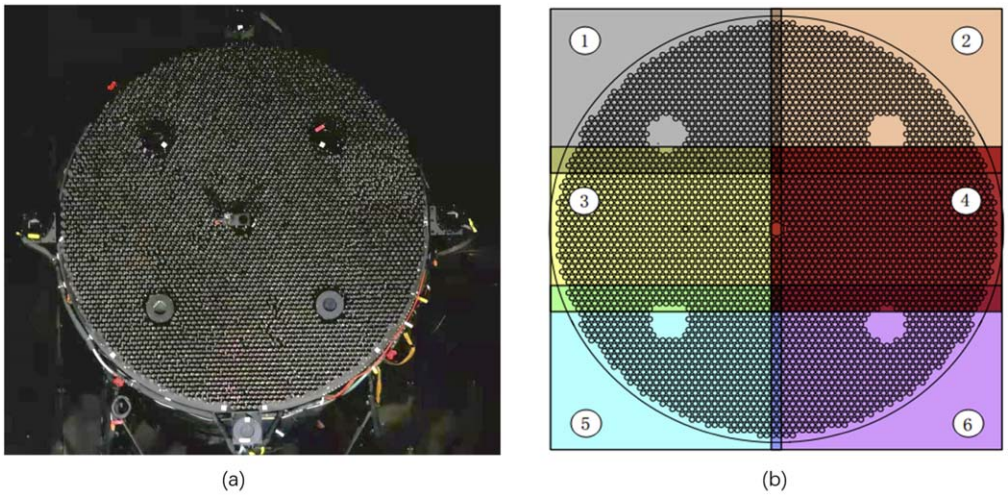

Figure 1. (a) LAMOST focal surface. (b) FOV division of six FVCs.

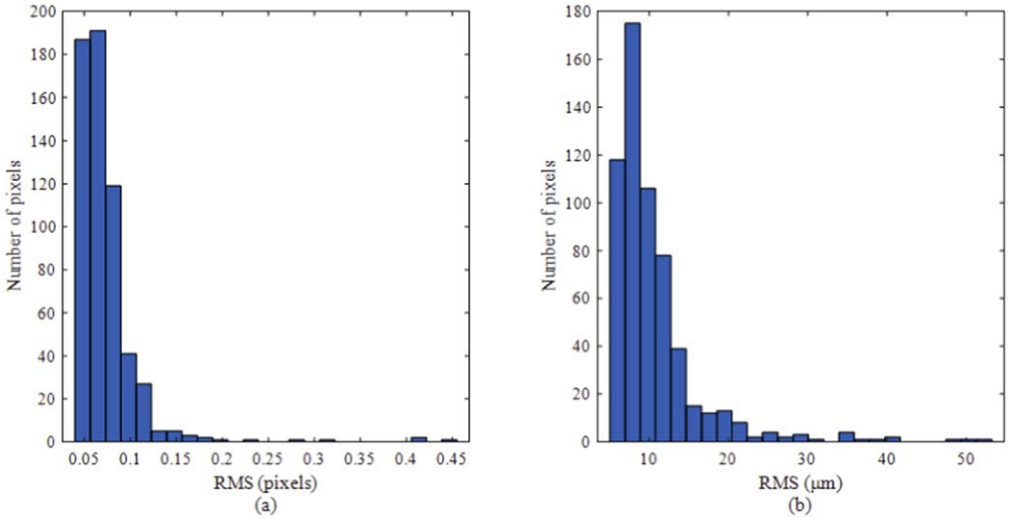

Figure 2. Calculation results for repeatability error using (a) average OF coordinates as theoretical coordinates (units: pixels) and (b) coordinates of machining holes in focal surface as theoretical coordinates (units: μm).

contained 587 working fibers, and so there were 587 input data points. Therefore, because there were far more input data points than the required number of calculation parameters, overfitting was not a concern (Tang et al. 2017). Finally, we calculated the repeatability error of each OF. The steps for calculating the repeatability error are as follows. First, the transformation relationship between objects and images is calculated by polynomial fitting, and each image is converted. The next step is to calculate the average position of an OF in the 1800 pictures and then calculate the distance between the OF and its average position in each picture. Finally, the root mean square (rms) value of all the distances is calculated as the repeatability error of that OF.

To assess how the OF positioning accuracy is affected by regarding the hole coordinates as the theoretical ones, we take the average positions of the OFs in the 1800 pictures as the theoretical coordinates to participate in polynomial fitting for comparison using the coordinates of the machining holes in the focal surface as the theoretical ones.

Figure 2 displays the results of the OF repeatability calculations. The horizontal axis represents the rms value and the vertical axis signifies the number of OFs. Figure 2(a) shows the fitting results using the average OF positions as the theoretical coordinates, and the units for the horizontal axis are pixels. Figure 2(b) depicts the fitting results regarding the coordinates of the machining holes in the focal plane as

Table 1
Repeatability Results for LAMOST OFs

No	Feature	Value
1	rms (fitting with average OF coordinates) [pixels]	7.32×10^{-2}
2	Scaled-up rms (fitting with average OF coordinates) [μm]	8.05
3	rms (fitting with hole coordinates) [μm]	10.62
4	Error magnification	31.93%

the theoretical coordinates, and the units for the horizontal axis are microns.

Table 1 gives the results of the LAMOST OF repeatability calculations. The values in the first and third rows are those of the mean all-OF rms in Figure 2, which are not directly comparable because of their different units. We convert the units of the data in the first row to microns; the conversion rate was obtained during previous polynomial fittings, and the result of the scale amplification is given in the second row of Table 1. We calculated the error magnification ratio using the hole coordinates and average OF coordinates. The expression for this is

$$\mathrm{EMR} = \frac{\mathrm{RMS(hole)} - \mathrm{RMS(OF)}}{\mathrm{RMS(OF)}} \times 100\% \qquad (2)$$

where rms(hole) is the rms using hole coordinates as the theoretical coordinates, rms(OF) is the rms using the average OF positions as the theoretical coordinates and EMR is the error magnification ratio.

The rms value obtained when fitting using the average OF coordinates was 0.0732 pixels, which equates to 8.05 μm. The rms value obtained when fitting using the hole coordinates was 10.62 μm, which is 31.93% more than the aforementioned rms. To verify our experimental results, we performed the same experiment in the laboratory using an accurately machined standard target.

2.2. Repeatability Experiment with Standard Target

To verify that using more-accurate theoretical coordinates in the polynomial fitting gives higher repeatability in positioning accuracy, we used a standard target with more-accurate theoretical coordinates in a controlled experiment. We performed repeatability experiments on the standard target in the laboratory to analyze its error. The standard target was an etched lattice with 4000 light spots, and the machining accuracy was ± 1 μm.

We again employed a 6k $\times$ 8k CMOS camera to shoot for 30 minutes, once per second, with a total of 1800 images taken. The distance between the camera and the standard target was 20 m. In an environment with no external light, we back-illuminated the standard target to perform the repeatability experiment. To assess how the repeatability was affected by using different theoretical coordinates, we compared the standard target machining position coordinates and the average positions of the spots in the 1800 pictures as the theoretical coordinates in the polynomial fitting.

Figure 3 shows the repeatability calculation results. The horizontal axis represents the rms value and the vertical axis signifies the number of spots. Figure 3(a) features the fitting results using the average spot positions as the theoretical coordinates, and the units for the horizontal axis are pixels. Figure 3(b) displays the fitting results using the coordinates of the machining spots of the standard target as the theoretical coordinates, and the units for the horizontal axis are microns.

Table 2 gives the results of the standard spots' repeatability calculations. The values in the first and third rows are those of the mean all-spot rms in Figure 3, which are not directly comparable because of their different units. We convert the units of the data in the first row to microns; the conversion rate was obtained during previous polynomial fittings, and the result of the scale amplification is given in the second row of Table 2. We also calculated the error magnification ratio using the hole coordinates and average OF coordinates.

The rms value for the standard target with fitting using the average coordinates was 0.027 pixels, equating to 2.65 μm. The value obtained when fitting using the machining spots was 2.71 μm, and the error is magnified by 2.26%. This result verifies our conclusion in Section 2.1, namely that using more-accurate theoretical coordinates in the polynomial fitting gives higher repeatability accuracy. Therefore, to improve the accuracy of positioning, we need a standard target with which to measure positions accurately for use in the polynomial fitting.

Figure 4 shows the structure of the FF unit (Duan et al. 2020), on which up to nine FFs are installed. This unit can be installed on the focal surface like an OF positioner. Inside the unit is an LED light to illuminate the OFs. The unit can be coded by installing a different number of FFs to provide coding points for fast fiber positioning in the future. The sphere-mounted retro-reflectors (SMR) can be magnetically attached in front of the unit. For convenience of viewing the structure of the unit, we omit the SMR in Figure 4.

Figure 5 shows how we use the FF units, on which the SMR is installed. The FF units are installed on the focal surface using a transition fit in the same way as the OF units in LAMOST. The laser tracker is a portable three-dimensional (3D) large-size measuring system based on polar coordinates, which has a lot of advantages such as high accuracy, broad range and on-site measurement. The laser beam from the laser tracker tracks the SMR to measure the 3D position of the required point (Yan et al. 2008). We measure the position of a unit by a laser tracker precisely. The FF units are installed on the focal surface and are identified by the camera in the same way that the OF positioners are. The rest of this paper discusses how the

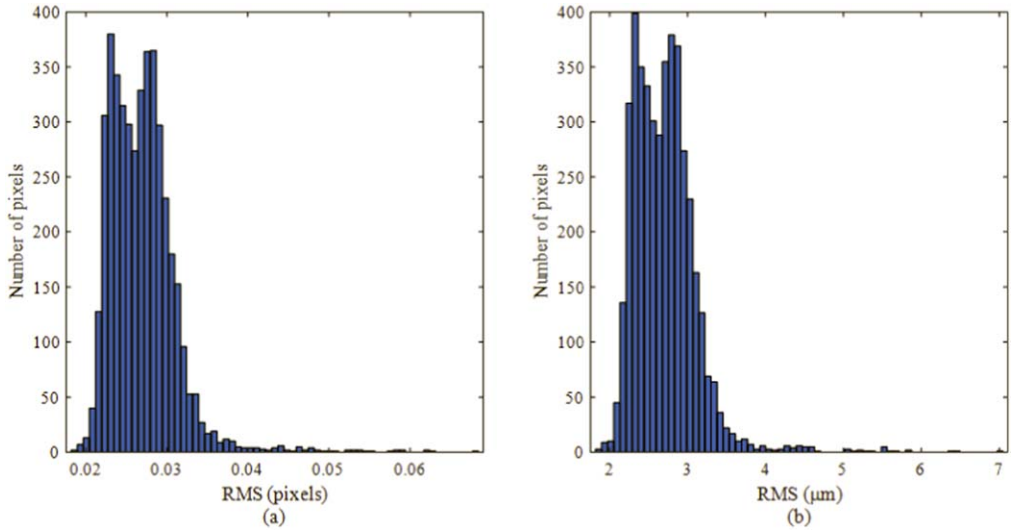

Figure 3. Calculation results for repeatability error with standard target using (a) average coordinates as theoretical coordinates (units: pixels) and (b) coordinates of machining spots as theoretical coordinates (units: μm).

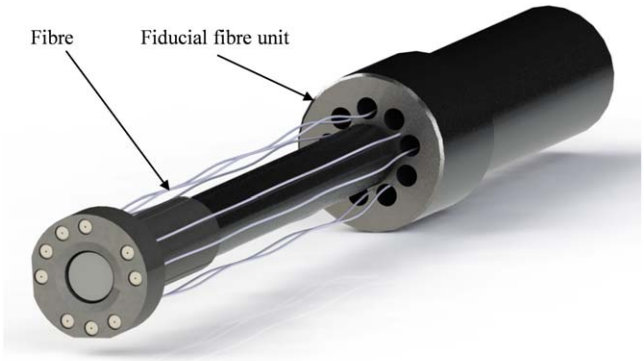

Figure 4. Structure of an FF unit.

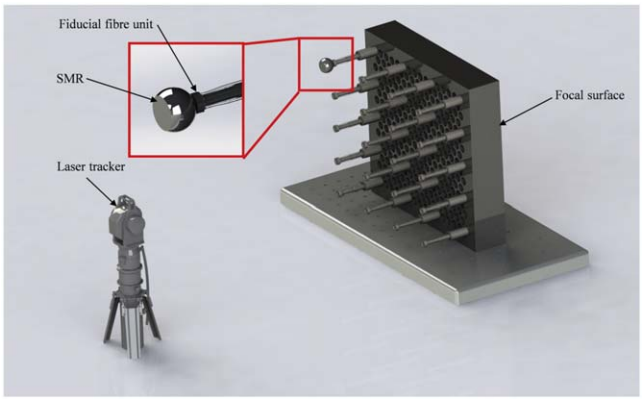

Figure 5. FF units installed on the focal surface, with one FF unit equipped with an SMR. The positions of the FF units are measured by a laser tracker.

Table 2
Experimental Repeatability Results for Standard Target

No	Feature	Value
1	rms (fitting with average coordinates) [pixels]	7.32×10^{-2}
2	Scaled-up rms (fitting with average coordinates) [μm]	2.65
3	rms (fitting with spot coordinates) [μm]	2.71
4	Error magnification	2.26%

number and distribution of FF units influence the repeatability error.

3. Number of Fiducial Fibers

During closed-loop detection, the FVCs shoot both the FF units and the working OFs simultaneously, and there are various errors that can affect the perceived positions of the FF units and working OFs. Using the coordinates of the FFs to perform polynomial fitting, we know that the more input points there are, the better the fitting. Therefore, we analyze how the number of FFs influences the fitting, and we calculate the repeatability error with different numbers of FFs.

3.1. Influence of Number of Fiducial Fibers

To explore how the number of FFs influences the repeatability error of shooting, a camera FOV is determined. Taking the FOV of FVC5 as an example and simulating using MATLAB, all the OFs are given different random and systematic errors. Increasing the number of FFs from 30 to 300, a fourth-order polynomial is used to simulate and calculate the repeatability error.

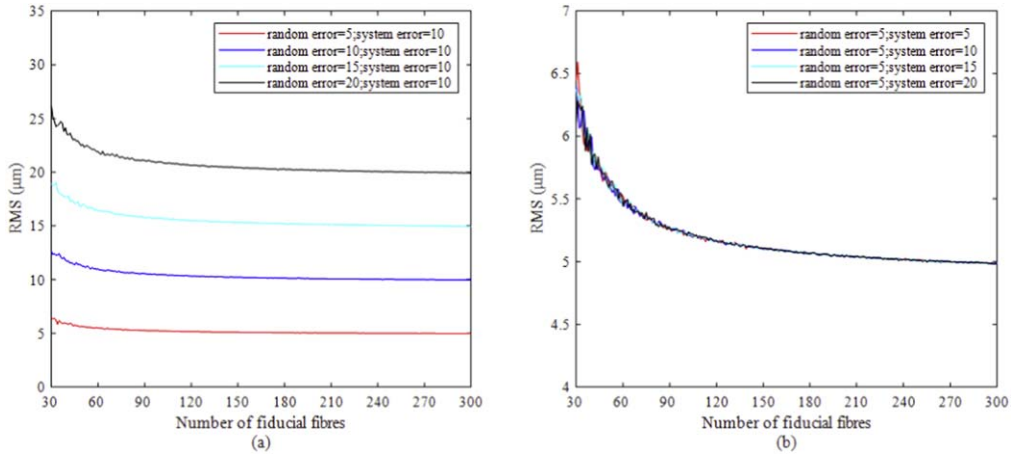

Figure 6. Relationship between number of FFs and repeatability error under different (a) random errors and (b) systematic errors.

Figure 6 shows the relationship between the number of FFs and the repeatability error. The horizontal axis represents the number of FFs, which are distributed randomly 100 times under the corresponding errors given in Figure 6. The symbols of each simulation plot are in the upper right corner of the graph, whereupon the rms value of the distribution with the smallest repeatability error is plotted on the vertical axis. Figure 6(a) depicts how the number of FFs affects the rms under different random errors (in microns), and Figure 6(b) shows the same but under different systematic errors. The random error is the random displacement error in two-dimensions given to each fiber in a single image, while the systematic error is the overall displacement error of all fibers in a single image.

The experimental results indicate that using more FFs (i) reduces the systematic error, (ii) gives a smaller final error but (iii) does not reduce the random error. The more FFs there are, the closer the final error is to the given random error, but using too few FFs gives a huge rms.

3.2. Research on Number of Fiducial Fibers

Figure 7 shows the error amplification percentage of different numbers of FFs. To determine the number of FFs, we calculated the error amplification percentage of different numbers of FFs in the case of Figure 6(b). The calculation formula for this is

$$\mathrm{EAP} = \frac{\mathrm{RMS} - 5}{\mathrm{RMS}} \times 100\% \tag{3}$$

where EAP is the error amplification percentage and rms is the value in Figure 6(b). Generally, the rms of the LAMOST OFs is 5–10 μm. If we assume that the error amplification is less than 10%, then the amplification error can be controlled to 0.5–1 μm, thereby ensuring the OF positioning accuracy. In Figure 6, no fewer than 58 FFs are needed to meet the requirements, so we chose to use 60 FFs for the subsequent distribution studies.

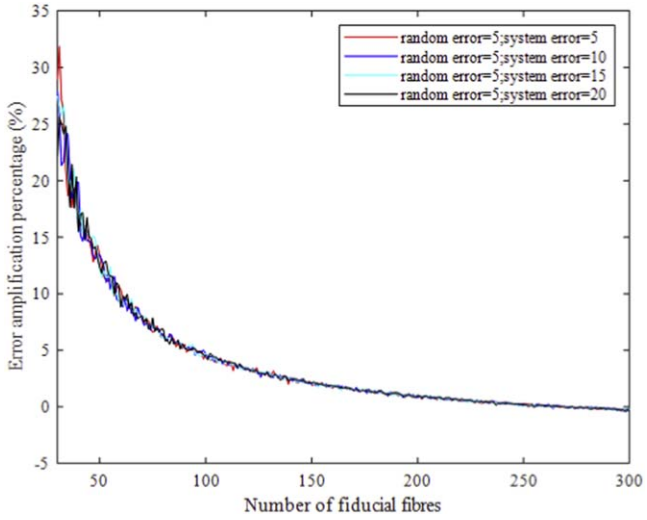

Figure 7. Error amplification percentages for different numbers of FFs.

4. Distribution of Fiducial Fibers

Having determined the number of FFs, we now explore how their distribution influences the repeatability error. Taking FVC5 as an example, the distribution is not a regular symmetrical one because the working OFs in the camera FOV are arranged in a fan shape with a hole in the center. Therefore, we seek a reasonable FF distribution in this irregular shape.

4.1. Influence of Distribution of Fiducial Fibers

Using MATLAB for the simulation calculations, we distributed 60 FFs randomly in the FOV of FVC5. Each fiber

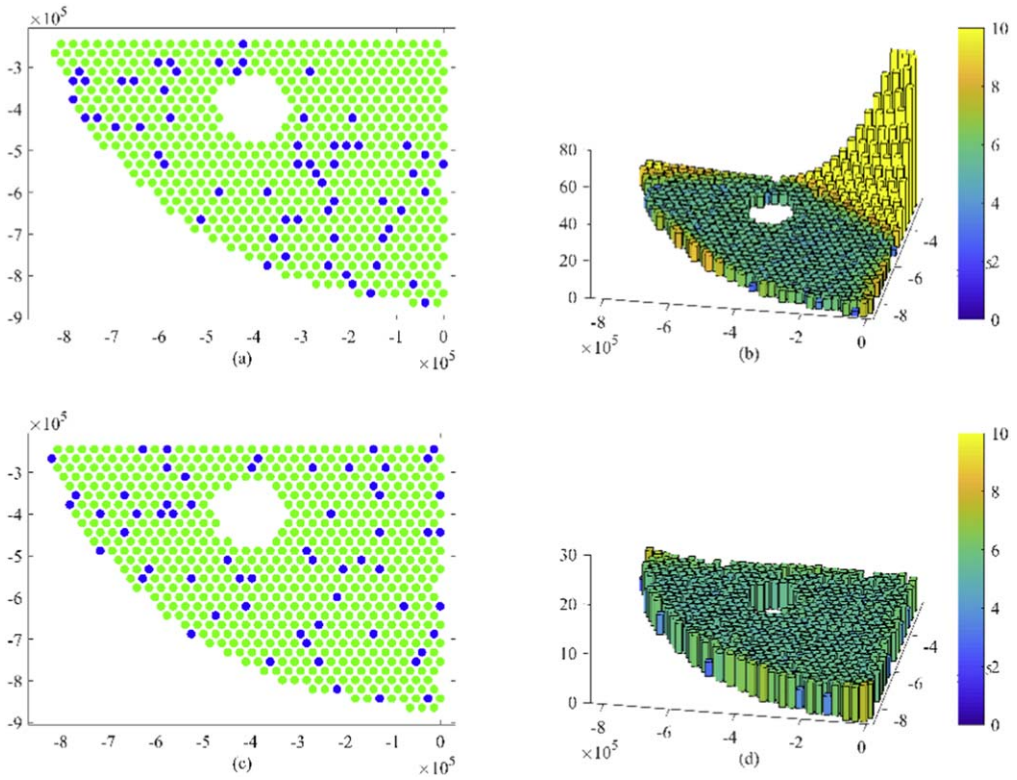

Figure 8. (a) Distribution with largest rms from 10,000 distributions, where green dots are working OFs and blue dots are FFs. (b) rms histogram for all fibers in (a) (units: μm). (c) Distribution with smallest rms from 10,000 distributions. (d) rms histogram for all fibers in (c) (units: μm).

was given a random error of 5 μm but no systematic error. We repeated the random distribution 10,000 times and found the ones with the largest and smallest rms values for comparison.

Figure 8(a) depicts the FF distribution with the largest rms, and Figure 8(b) shows the corresponding rms histogram for all the OFs. The average rms value was 5.73 μm, which is 14.6% larger than the given random error of 5 μm. Figure 8(c) displays the FF distribution with the smallest rms value, and Figure 8(d) features the corresponding rms histogram for all the OFs. The average rms value was 5.42 μm, which is 8.4% larger than the given random error of 5 μm.

In Figure 8(b), the rms value increases significantly in the area with no FF coverage at the edge, because this area is under-fitted in the polynomial fitting. Also, from matrix theory, if neighboring FFs are closer together, then the direct linear correlation between the corresponding columns will be greater in the high-order matrix fitting, and the parameter matrix formed by the reference points will be more likely to cause singularity, which will lead to local overfitting. According to the law of polynomial fitting, the more uniform the FF distribution is, the smaller the repeatability error. Furthermore, to avoid under-fitting of the edge part, the FF distribution must surround the working OFs.

4.2. Research on Distribution of Fiducial Fibers

To explore a method for distributing the FFs as evenly as possible under the existing conditions, herein we compare several methods to quantify whether the FFs are distributed uniformly, and we calculate the correlation between the results of these methods and the repeatability error. To assess the distribution uniformity, we use the random-point method, the coverage method and the Voronoi-diagram method (Aurenhammer 1991).

1. Random-point method. From a statistical perspective (Fang et al. 1994), we distribute 1000 points randomly in the working-OF area and calculate the distance from each point to the nearest FF, a total of 1000 distances. We then use the standard deviation of all these distances as the basis for assessing the uniformity of the FF distribution. However, the results of each distribution are random and the results are not unique.
2. Coverage method. We pre-set a coverage radius for each FF and calculate the coverage percentage of FFs with different distributions. Figure 9(a) displays an FF distribution, where the green dots are the working OFs and the blue dots are the FFs. As shown in Figure 9(b), each FF has a circular coverage with a pre-set coverage

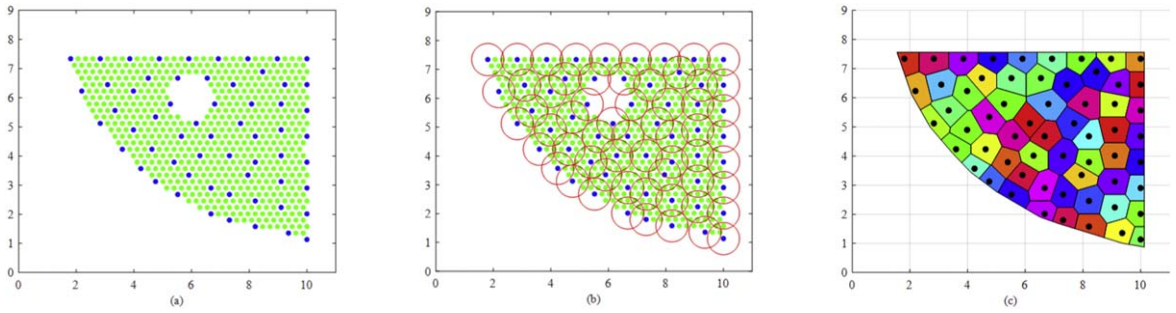

Figure 9. (a) Example of FF distribution, where green dots are working OFs and blue dots are FFs. (b) Schematic of coverage method. (c) Schematic of Voronoi-diagram method.

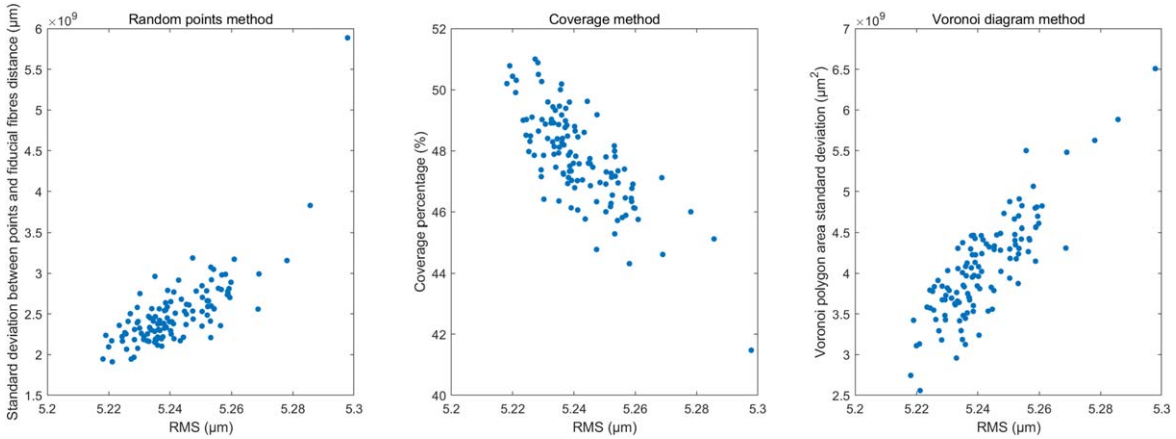

Figure 10. Relationships between results of the three methods and repeatability rms.

radius. The coverage radius of the FFs is determined by the active range of the OFs. The sum of the circular coverage area of all FFs is equal to the active range area of the OFs. An area that is repeatedly covered by multiple FFs is considered to be covered only once. The coverage result is the percentage of the area covered by FFs in the area of all OF active areas. In this method, the coverage result for each distribution is unique.

3. Voronoi-diagram method. This is used widely to assess distribution uniformity (Wu et al. 2007). The Voronoi polygons are connected by the circumscribed circle center of each triangle in the Delaunay algorithm. The working-OF area is divided into polygons equal to the number of FFs. As depicted in Figure 9(c), each polygon contains an FF. We take the area of Voronoi polygons as the FF coverage area and calculate the standard deviation of all polygon areas as the basis for assessing the distribution uniformity: the smaller the standard deviation, the more uniform the distribution. The standard deviation of each distribution is unique.

We used MATLAB for the simulation calculations, giving each fiber a random error of 5 μm but no systematic error. The FFs were distributed randomly 120 times to calculate the fiber repeatability rms. Figure 10 shows the simulation results in the form of the corresponding relationships between the results of the three methods and the fiber repeatability rms.

Table 3 gives the results of the correlation analysis between the results of the three methods and rms, and the Voronoi method has the largest Pearson correlation coefficient with rms, which is 0.839 and has a strong correlation. Sig. (2-tailed) represents significance (Balazs et al. 2006), and a Sig. (2-tailed) value less than 0.01 indicates that the correlation coefficient is statistically significant, so we used the Voronoi method as the basis for assessing the distribution uniformity.

Herein, the problem of the uniform distribution is described as an optimization problem, and the optimal or approximately optimal solution of the problem is solved by PSO. This is a population-based optimization tool inspired by the natural social behavior of certain organisms, such as birds flocking and fish schooling, and it has been used successfully in many areas (Wang et al. 2020). Herein, the optimal FF positions are determined by implementing PSO and the adaptability function based on the Voronoi diagram. The computational complexity is controlled by only one parameter, namely the FF distribution.

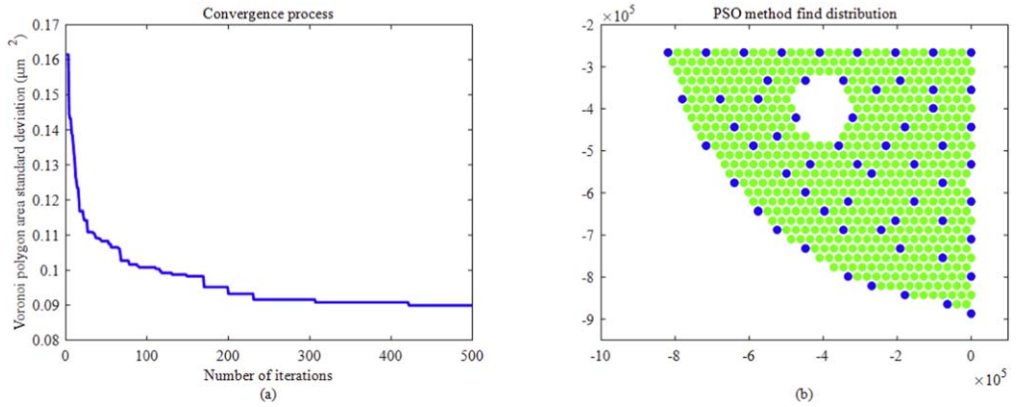

Figure 11. (a) Convergence process of PSO. Horizontal axis: number of iterations; vertical axis: standard deviation of Voronoi polygons. (b) Distribution result of final convergence.

Table 3
Experimental Repeatability Results for Standard Target

		Random Points Method	Coverage Method	Voronoi Method	rms
Random-point method	Pearson correlation coefficient	1	−0.830	0.775	0.760
	Sig. (2-tailed)		0.000	0.000	0.000
	Number of cases	120	120	120	120
Coverage method	Pearson correlation coefficient	−0.830	1	−0.809	−0.758
	Sig. (2-tailed)	0.000		0.000	0.000
	Number of cases	120	120	120	120
Voronoi method	Pearson correlation coefficient	0.775	−0.809	1	0.839
	Sig. (2-tailed)	0.000	0.000		0.000
	Number of cases	120	120	120	120
rms	Pearson correlation coefficient	0.760	−0.758	0.839	1
	Sig. (2-tailed)	0.000	0.000	0.000	
	Number of cases	120	120	120	120

Taking the FOV of FVC5 as an example, we selected 60 FFs to design the distribution in the working-OF area. Based on the standard deviation of the Voronoi polygonal area, the distribution was found using PSO. First, to prevent the edge of the fiber area from being under-fitted, we distributed 26 FFs on the edge and then performed PSO. Before the calculation, we set the initial population number as 500, the number of iterations as 1000, the dimension as 34, the inertia weight as 0.5, the self-learning factor as 0.3 and the group learning factor as 0.3. Figure 11(a) shows the iterative process and Figure 11(b) displays the final convergent FF distribution.

After this, we tested the distribution found by PSO. We gave each fiber a random error of 5 μm but no systematic error. Because of the randomness of the error, we calculated a total of 1000 times to assess the repeatability of the rms value of the simulation.

Figure 12 depicts the simulation results. The maximum error amplification percentage was 7.13%, the minimum was 5.99% and the mean was 6.53%. The simulation results affirm that choosing a good distribution reduces the error magnification further.

5. Conclusions

This paper discusses FFs used in camera measurement in the OF positioning system and demonstrates that FFs are necessary for OF positioning. We proposed a method to determine quantity of FFs through simulation experiments. We ascertained through experimentation that the more uniformly distributed FFs will get better repeatability error of OFs. Then we conducted a correlation analysis between the repeatability error of OFs and the standard deviation of the Voronoi polygon area. The experimental results showed that the standard deviation of the Voronoi polygon area is positively correlated with the repeatability error of OFs. Finally, we use PSO to find a reasonable distribution of FFs.

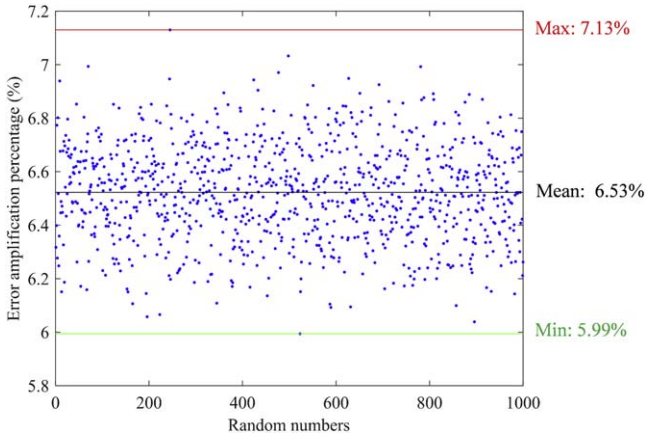

Figure 12. Test results for final distribution. Horizontal axis: number of simulations; vertical axis: error amplification percentage.

In this paper, the specific analysis and experimental simulation provide a practical optimization method for the number and distribution of FFs for the LAMOST focal surface. The constraint condition for a uniform distribution of FFs, which is affected by the installation of guide CCD and other devices on the LAMOST focal surface, is optimized. The whole process has good practical applications. If FFs cannot be distributed in certain regions on the focal surface of different survey telescopes, the number and distribution of FFs can be recalculated by referring to the method in this paper. This paper provides a design reference for the FF distribution on the LAMOST upgrade or other large-scale spectral survey telescopes with more than thousands of OFs in the future and is suitable for obtaining the optimal solution of the number of FFs and the distribution under different constraints.

Acknowledgments

Funding for the research was provided by Cui Xiangqun's Academician Studio. Guoshoujing Telescope (the Large Sky Area Multi-Object Fiber Spectroscopic Telescope, LAMOST) is a National Major Scientific Project built by the Chinese Academy of Sciences. Funding for the project has been provided by the National Development and Reform Commission. LAMOST is operated and managed by the National Astronomical Observatories, Chinese Academy of Sciences.

Data Availability

The data underlying this article will be shared on reasonable request to the corresponding author.

ORCID iDs

Zeng-Xiang Zhou, https://orcid.org/0000-0002-3050-5822

References

Aghamousa, A., Aguilar, J., Ahlen, S., et al. 2016, arXiv:1611.00037
Aurenhammer, F. 1991, ACM Comput. Surv., 23, 345
Balazs, L. G., Hetesi, Z., Regaly, Z., et al. 2006, AN, 327, 917
Cui, X. Q., Zhao, Y. H., Chu, Y. Q., et al. 2012, RAA, 12, 1197
Duan, S., Zuo, J., Li, M., et al. 2020, Proc. SPIE, 11445, 1102
Fang, K. T., Wang, Y., & Bentler, P. M. 1994, StaSc, 9, 416
Fisher, C., Morantz, C., Braun, D., et al. 2014, Proc. SPIE, 9151, 91511Y
Fisher, C. D., Braun, D. F., Kaluzny, J. V., et al. 2012, Proc. SPIE, 8450, 845017
Horler, P., Kronig, L., Kneib, J. P., et al. 2018, MNRAS, 481, 3070
Hu, H., Chao, Z., Li, W., et al. 2006, Proc. SPIE, 6269, 62693A
Hu, H., Wang, J., Liu, Z., Zhou, Z., & Chu, J. 2016, Proc. SPIE, 9912, 991259
Hu, H., Wang, J., Liu, Z., Zhou, Z., & Chu, J. 2018, Proc. SPIE, 10706, 107065U
Hu, H., Xing, X., Chao, Z., & Li, W. 2003, Proc. SPIE, 4837, 548
Liu, Z., Chao, Z., Hu, H., Wang, J., & Chu, J. 2011, Proc. SPIE, 8149, 81490H
Pérez-Calpena, A., Cedazo, R., Sánchez, E., Gomez-Cambronero, P., & Iglesias-Páramo, J. 2018, Proc. SPIE, 10706, 107062C
Schubnell, M., Ameel, J., Besuner, R. W., Gershkovich, I., & Weaverdyck, C. 2016, Proc. SPIE, 9908, 990892
Tang, Z. W., von Gioi, R. G., Monasse, P., & Morel, J. M. 2017, ITIP, 26, 2694
Wang, J. Y., Guo, Y. M., Kong, L., et al. 2020, MNRAS, 496, 5126
Wu, C. H., Lee, K. C., & Chung, Y. C. 2007, Comput. Commun., 30, 2744
Xing, X., Chao, Z., Du, H., & Li, W. 1998, Proc. SPIE, 3352, 839
Yan, Y. G., Ouyang, J. F., Liu, W. L., & Xia, F. 2008, Optical Design and Testing III, Pts 1 and 2, 2, 6834
Zhao, K., Liu, Z., Hu, H., et al. 2018a, Proc. SPIE, 10702, 1070277
Zhao, K., Liu, Z., Hu, H., Wang, J., & Zhou, Z. 2018b, Proc. SPIE, 10700, 107002A
Zhou, Z., Liu, Z., Hu, H., et al. 2016, Proc. SPIE, 9912, 991258